Geophys. J. R. astr. Soc. (1982) **68**, 675–688

Lateral heterogeneity in the seismic structure of the oceanic crust inferred from velocity studies in the Bay of Islands ophiolite, Newfoundland

Nikolas I. Christensen *Department of Geological Sciences and Graduate Program in Geophysics, University of Washington, Seattle, Washington 98195, USA*

Matthew H. Salisbury *Deep Sea Drilling Project and Geological Research Division, Scripps Institution of Oceanography, La Jolla, California 92093, USA*

Received 1981 June 26; in original form 1980 October 17

Summary. In the Bay of Islands ophiolite complex of Western Newfoundland, Lower Ordovician crust and upper mantle are exposed in four massifs. Two of these, the Blow-Me-Down and North Arm massifs, contain complete or nearly complete ophiolite successions ranging from clastic sediments at the top, through pillow basalts, sheeted dykes, gabbros, and peridotites at the base. The detailed velocity structure of the North Arm massif has been reconstructed from compressional and shear wave velocity measurements to confining pressures of 6 kbar and low pore pressures for 125 cores collected from 43 sites of known stratigraphic level and is compared with the previously determined seismic structure of the Blow-Me-Down massif. Within the upper 2 km of North Arm, compressional wave velocities increase from 5.0 to 7.0 km s^{-1} and shear wave velocities increase from 2.8 to 3.8 km s^{-1}. Velocities at this level in the Blow-Me-Down massif are higher due to the presence of pumpellyite. In both massifs, the top of layer 3 occurs within the sheeted dyke complex at a depth of approximately 1.5 km and marks the transition from greenschist to amphibolite facies metadolerites. High level gabbros and plagiogranites at depths of between 2 and 4 km are responsible for velocity inversions. In North Arm, Poisson's ratios at this depth are relatively high (0.31–0.34); whereas in Blow-Me-Down, abundant quartz-rich plagiogranites give rise to low Poisson's ratios (0.25–0.27). The lowest crustal unit in North Arm, which consists primarily of gabbro and amphibolite, has average compressional and shear wave velocities of 7.0 and 3.8 km s^{-1}, respectively. Within this section (4–6 km) the velocities decrease slightly with increasing depth in North Arm, but increase abruptly at 5.5 km depth in Blow-Me-Down. In the North Arm massif, the transition from crust to mantle is rather gradual due to the presence of a relatively thick mixed zone of gabbro and ultramafics.

1 Introduction

The Bay of Island ophiolite complex of Western Newfoundland is composed of four major massifs (Fig. 1): Table Mountain, North Arm Mountain, Blow-Me-Down Mountain, and the

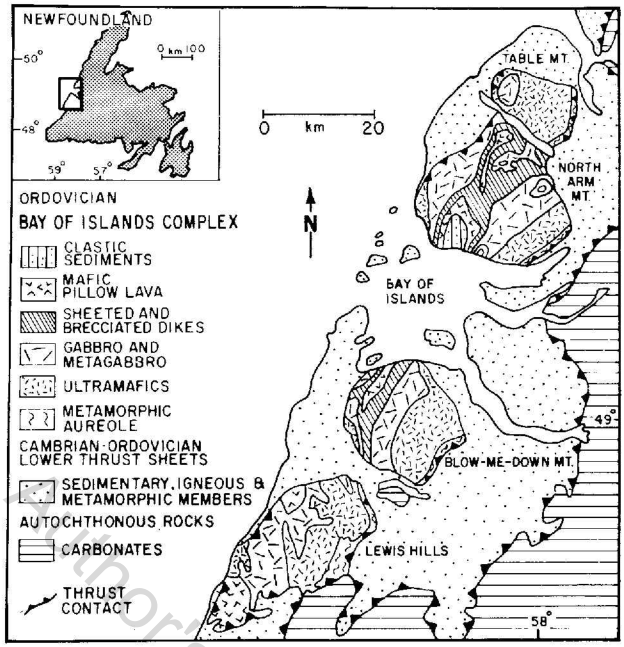

Figure 1. Geology and location of the four massifs from the Bay of Islands complex, Newfoundland, after Williams (1971).

Lewis Hills. Exposures are excellent and mapping by Smith (1958), Williams & Malpas (1972) and Williams (1973) has found an ophiolite sequence consisting from the top downward of clastic sediments, pillow basalts with intercalated sediments and flows, sheeted dykes, gabbros and ultramafics. Of the four massifs, only one, North Arm Mountain, appears to be complete. The sedimentary unit and uppermost levels of basalt have been removed by erosion from the Blow-Me-Down and Lewis Hills massifs, and in Table Mountain only the lower gabbroic and ultramafic units remain (Smith 1958).

These massifs are interpreted as Lower Ordovician oceanic crust and upper mantle (Stevens 1970; Church & Stevens 1971; Williams 1971; Mattinson 1976; Jacobsen & Wasserburg 1979), possibly originating within an opening and closing proto-Atlantic Ocean (Wilson 1966). In an earlier paper (Salisbury & Christensen 1978), we reconstructed the seismic velocity structure of a traverse through the Blow-Me-Down massif from laboratory measurements of compressional and shear wave velocities at hydrostatic confining pressures appropriate for the oceanic crust. It was concluded that the measured velocity structure was similar to that of normal oceanic crust as determined by marine seismic refraction measurements. Of major significance: (1) the layer 2–3 boundary was found to coincide with the greenschist facies–epidote-amphibolite facies boundary within the sheeted dykes; (2) a 7.4 km s^{-1} basal crustal layer consisting of interlayered olivine gabbro, troctolite, and plagioclase peridotite was observed in the compressional wave velocity profile; (3) a velocity inversion associated with plagiogranite was observed at intermediate levels in layer 3; and (4) the Mohorovičić discontinuity correlated with a sharp transition from gabbro to dunite and peridotite.

The present investigation presents detailed compressional (V_p) and shear (V_s) wave velocity columns and profiles of Poisson's ratio (σ) and density (ρ) for the North Arm massif. The study was undertaken for the following reasons: (1) There is considerable interest in the extent of lateral variability within various levels of the oceanic crust (Christensen & Salisbury 1975; Orcutt *et al.* 1975). Although the exact spatial separation of the Blow-Me-Down and North Arm massifs at their time of formation is uncertain, it is probable that they originated within a few tens of kilometres of one another. Thus, a comparison of their velocity structures provides information on lateral variations in oceanic crustal seismic structure. (2) Detailed studies of the seismic anisotropy of the ultramafics from the North Arm massif (Christensen & Salisbury 1979) have shown a symmetry and magnitude similar to those observed in the oceanic upper mantle. The crustal velocity profiles presented here thus complete the velocity structure of the massif. (3) Within the Blow-Me-Down massif, part of the upper basalt section is stripped by erosion. The sediment–basalt contact of the North Arm massif, however, is well exposed along a tributary south of Lower Crabb Brook, making it possible to have more precise stratigraphic control for the upper portion of the velocity columns. (4) In subsequent mapping and laboratory investigations, we have found evidence for the presence of a major fault separating the gabbro and ultramafics within the Blow-Me-Down massif. Because of the presence of interlayered ultramafics within the lower gabbro section, we believe the faulting has not produced significant stratigraphic thinning of the crustal section. Within the North Arm massif, on the other hand, the mafic–ultramafic contact is gradational and thus intact.

2 Procedures and data

The approaches we have taken for sample collection, preparation and velocity measurement are essentially the same as those described in detail by Salisbury & Christensen (1978).

The samples were collected at closely spaced intervals along the traverses shown in Fig. 2. At each site the samples were field oriented so that cores for physical property measurements could be taken with reference to such features as bedding, dyke orientation, cumulate layering, tectonite banding and foliation. Three cores with mutually perpendicular axes were taken from each sample. Within layered or banded units, two of these (cores 1 and 2 in Table 1) were aligned parallel to the plane of layering and the third was cut perpendicular to layering. The core diameters were 1.27, 1.90 or 2.54 cm and the lengths varied from 2.6 to 6.8 cm, with the larger cores cut from the coarser-grained gabbros. Each core was first weighed dry, then water saturated and reweighed saturated. The bulk densities were then calculated from the core dimensions and the wet and dry weights. Effective porosities were obtained from the wet and dry bulk densities.

Prior to the velocity measurements, the saturated cores were wrapped with an inner layer of 100 mesh screen and an outer layer of copper foil. The screen serves to provide space for pore water expelled during compression, thus maintaining relatively low pore pressures at high confining pressures. A similar technique was used for our earlier velocity measurements for Bay of Islands samples (Salisbury & Christensen 1978). Transducers with resonant frequencies of 2 MHz and backing electrodes were placed on the core ends and then covered with gum rubber tubing to hold the assembly in place and prevent the pressure medium from entering the rock pore spaces. Thus, during runs, the pore spaces of the samples were water saturated rather than saturated with the pressure medium (hydraulic oil). Using the pulse transmission method described by Birch (1960), velocities were measured at 0.2 kbar intervals between atmospheric pressure and 1.0 kbar, and at 1.0 kbar intervals between 2.0 and 6.0 kbar. The velocities are estimated to be accurate to better than 1 per cent.

Compressional and shear wave velocities, wet bulk densities, effective porosities and Poisson's ratios calculated from the mean velocities at *in situ* confining pressures are presented in Table 1. Typical velocity–pressure curves are shown in Fig. 3 for a metadolerite

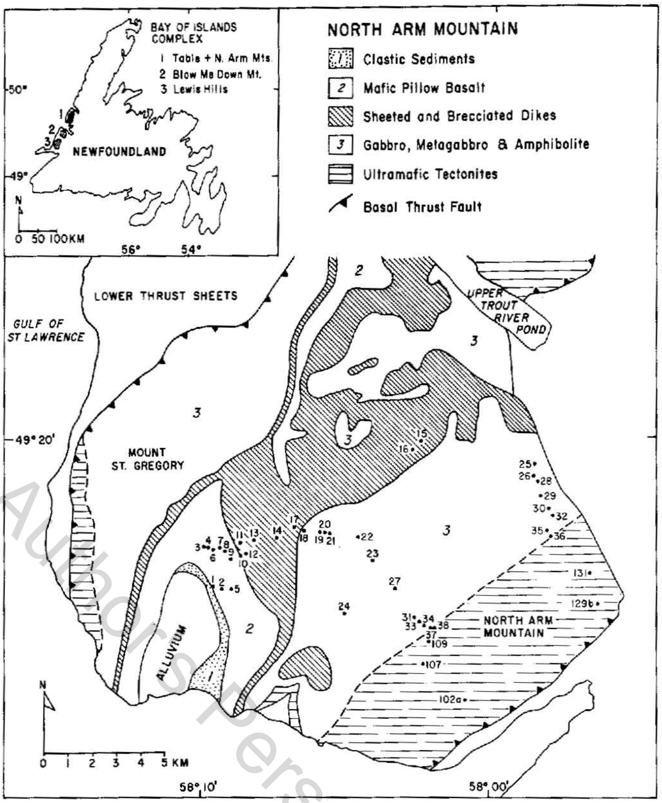

Figure 2. Geology, after Williams (1971), of the North Arm massif and locations of samples selected for velocity, porosity and density measurements.

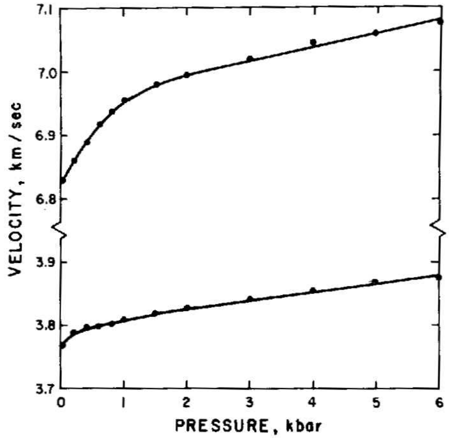

Figure 3. Compressional (V_p) and shear (V_s) wave velocities versus confining pressure for a metadolerite dyke rock.

Table 1. Compressional (*P*) and shear (*S*) wave velocities for samples from the North Arm massif at confining pressures (P_c) appropriate to the seafloor.

Sample	Lithology	Depth, km	Pc, kbar	Density, g/cm^3 1	Density 2	Density 3	Density Mean	% Porosity Mean	Mode	Velocity, km/s 1	Velocity 2	Velocity 3	Velocity Mean	Poisson's Ratio
1	Metabasalt	0.04	0.5	2.69	2.71	2.69	2.70	0.8	P	5.64	5.53	5.66	5.61	0.30
									S	3.02	2.93	3.00	2.98	
2	Metabasalt	0.18	0.6	2.68	2.70	2.68	2.69	1.1	P	5.55	5.72	5.55	5.61	0.32
									S	2.90	2.93	2.93	2.92	
3	Metabasalt	0.32	0.6	2.80	2.79	2.79	2.79	3.0	P	5.33	5.18	5.44	5.32	0.30
									S	2.88	2.81	2.85	2.85	
4	Metabasalt	0.39	0.6	2.65	2.65	2.64	2.65	3.2	P	5.41	5.12	5.31	5.28	0.29
									S	2.95	2.80	2.84	2.86	
5	Metabasalt	0.46	0.6	2.78	2.73	2.81	2.77	0.9	P	5.73	5.60	5.85	5.73	0.31
									S	3.07	2.90	3.06	3.01	
6	Metabasalt	0.51	0.7	2.74	2.74	2.70	2.73	3.2	P	5.48	5.51	5.44	5.48	0.31
									S	2.85	2.83	2.88	2.85	
7	Metabasalt	0.65	0.7	2.84	2.85	2.83	2.84	3.3	P	5.39	5.53	5.30	5.41	0.31
									S	2.83	2.90	2.76	2.83	
8	Metabasalt	0.72	0.7	2.86	2.85	2.85	2.85	1.9	P	5.77	5.75	5.70	5.74	0.31
									S	3.07	3.03	3.01	3.04	
9	Metabasalt	0.80	0.7	2.72	2.71	2.69	2.71	1.2	P	5.55	5.70	5.69	5.65	0.30
									S	2.92	3.06	3.03	3.00	
10	Metadolerite	0.97	0.8	2.76	-	2.76	2.76	2.9	P	6.00	-	6.25	6.13	0.33
									S	3.03	-	3.22	3.13	
11	Metadolerite	1.05	0.8	2.84		2.93	2.89	1.7	P	6.15	-	6.05	6.10	0.29
									S	3.43	-	3.38	3.41	
12	Metadolerite	1.19	0.8	2.89	2.94	2.89	2.91	1.4	P	6.44	6.64	6.47	6.52	0.32
									S	3.33	3.36	3.35	3.35	
13	Metadolerite	1.40	0.9	2.91	2.88	2.89	2.89	0.9	P	6.75	6.61	6.71	6.69	0.31
									S	3.64	3.51	3.43	3.52	
14	Metadolerite	1.74	1.0	2.89	2.90	2.90	2.90	0.5	P	6.80	6.63	6.76	6.73	0.28
									S	3.76	3.72	3.72	3.73	
15	Metadolerite	1.76	1.0	2.87	2.86	2.90	2.88	0.6	P	6.70	6.89	6.73	6.77	0.29
									S	3.63	3.73	3.67	3.68	
16	Metadolerite	1.85	1.0	2.93	2.92	2.97	2.94	1.0	P	6.83	6.83	6.94	6.87	0.30
									S	3.64	3.60	3.77	3.67	
17	Metadolerite	2.1	1.1	2.90	2.90	2.92	2.91	0.1	P	6.90	7.07	6.91	6.96	0.29
									S	3.82	3.83	3.79	3.81	
18	Metagabbro	2.2	1.2	2.87	2.86	2.87	2.87	0.6	P	6.59	6.62	6.61	6.61	0.28
									S	3.61	3.65	3.65	3.64	
19	Metagabbro (altered)	2.7	1.3	2.71	2.70	2.67	2.69	0.6	P	6.46	6.32	6.35	6.38	0.31
									S	3.36	3.34	3.27	3.32	
20	Metagabbro (altered)	2.8	1.3	2.62	2.64	2.61	2.62	0.6	P	6.68	6.80	6.77	6.75	0.34
									S	3.34	3.25	3.39	3.33	
21	Metagabbro (altered)	2.9	1.3	2.78	2.74	2.81	2.78	0.9	P	6.40	6.38	6.44	6.41	0.31
									S	3.47	3.41	3.26	3.38	
22	Metagabbro	3.3	1.4	2.91	-	2.87	2.89	0.8	P	6.57	-	6.41	6.44	0.29
									S	3.53	-	3.53	3.53	
23	Gabbro	3.7	1.6	2.96	2.96	2.97	2.96	0.5	P	7.20	7.24	7.07	7.17	0.30
									S	3.87	3.83	3.73	3.81	
24	Gabbro	4.1	1.7	2.85	2.93	2.87	2.88	0.7	P	7.14	7.21	7.24	7.20	0.30
									S	3.85	3.91	3.77	3.84	
25	Amphibolite	4.4	1.8	2.96	2.96	2.95	2.96	1.0	P	6.77	6.76	6.74	6.76	0.27
									S	3.77	3.75	3.79	3.77	
26	Amphibolite	4.8	1.9	3.05	3.01	2.98	3.01	1.1	P	6.91	6.93	6.68	6.84	0.29
									S	3.80	3.78	3.73	3.77	
27	Gabbro	4.9	1.9	3.03	2.98	3.02	3.01	0.5	P	7.50	7.45	7.40	7.45	0.31
									S	3.97	3.89	3.90	3.92	
28	Amphibolite	5.0	1.9	2.97	3.00	3.01	2.99	0.4	P	6.94	6.99	6.96	6.96	0.29
									S	3.84	3.72	3.79	3.78	
29	Gabbro	5.4	2.0	2.96	2.98	2.97	2.97	0.8	P	6.91	6.65	6.79	6.78	0.28
									S	3.76	3.69	3.72	3.72	
30	Gabbro	5.6	2.1	2.92	2.97	2.95	2.95	0.5	P	6.90	7.13	7.11	7.05	0.31
									S	3.56	3.77	3.83	3.72	
31	Wehrlite	5.9	2.2	3.09	3.08	3.07	3.08	0.4	P	7.16	7.16	7.20	7.17	0.34
									S	3.37	3.56	3.56	3.50	
32	Gabbro	5.9	2.2	2.91	2.88	2.88	2.89	0.2	P	7.28	7.12	7.14	7.18	0.30
									S	3.96	3.78	3.80	3.85	
33	Peridotite (serpentinized)	6.0	2.2	2.98	2.97	3.01	2.99	0.3	P	7.09	6.86	6.70	6.88	0.33
									S	3.45	3.44	3.52	3.45	
34	Gabbro	6.2	2.3	2.80	2.77	2.77	2.78	0.2	P	7.09	7.11	7.15	7.11	0.35
									S	3.38	3.35	3.42	3.38	
35	Gabbro	6.3	2.3	-	2.92	2.92	2.92	0.4	P	-	7.08	7.15	7.11	0.28
									S	-	3.88	3.94	3.91	
36	Gabbro	6.4	2.3	2.96	2.95	2.91	2.94	0.2	P	7.16	7.12	6.92	7.06	0.31
									S	3.77	3.77	3.63	3.72	
37	Gabbro	6.4	2.3	2.97	2.97	2.96	2.97	0.1	P	7.19	7.15	7.19	7.18	0.30
									S	3.84	3.88	3.84	3.85	
38	Gabbro	6.5	2.4	2.99	2.95	2.97	2.97	0.2	P	7.46	7.39	7.56	7.47	0.37
									S	3.39	3.45	3.41	3.42	
109	Peridotite (serpentinized)	7.1	2.5	2.76	2.78	2.75	2.76	1.1	P	5.83	6.31	5.89	6.01	0.32
									S	2.96	3.15	3.30	3.14	
107	Peridotite (serpentinized)	7.5	2.7	2.60	2.63	2.58	2.60	1.7	P	5.42	5.82	5.85	5.70	0.34
									S	2.70	2.70	2.85	2.75	
131	Peridotite (serpentinized)	8.0	2.8	2.67	2.77	2.78	2.74	0.6	P	6.22	6.33	6.07	6.21	0.33
									S	3.15	3.09	3.03	3.09	
102a	Peridotite (serpentinized)	8.9	3.1	2.60	2.57	2.60	2.59	2.7	P	5.43	5.70	5.34	5.49	0.35
									S	2.78	2.68	2.64	2.70	
129b	Peridotite (serpentinized)	9.1	3.2	2.73	2.76	2.74	2.74	0.7	P	6.16	6.14	5.91	6.07	0.34
									S	3.02	3.02	3.00	3.01	

dyke (no. 17). The velocities presented in Table 1 were determined from similar velocity–pressure curves for pressures calculated from the geologically estimated thickness and density of the overlying rock column. An additional hydrostatic confining pressure of 0.5 kbar was added for all samples to account for the seawater and sediments originally overlying the section. This assumes an average water depth of approximately 5 km.

Velocities in water-saturated oceanic rocks show less change with increasing confining pressure than do the velocities of dry samples (Christensen & Salisbury 1975). That the appropriate *in situ* velocities are therefore not highly sensitive to depth estimation is illustrated by the velocities in Fig. 3: at pressures greater than the seafloor average (0.5 kbar), an error of 0.1 km s^{-1} in velocity requires a minimum error in hydrostatic pressure estimation of 1.6 kbar for compressional waves and 6.5 kbar for shear waves. This corresponds to errors in depth estimation of 6 and 21 km for compressional and shear waves, respectively.

3 Petrology and seismic structure of the North Arm massif

The petrology and structural geology of various portions of the Bay of Islands ophiolite have been described in several papers (e.g. Cooper 1936; Smith 1958; Church & Stevens 1971; Williams 1971, 1973, 1975; Williams & Malpas 1972; Karson & Dewey 1978; Salisbury & Christensen 1978; Christensen & Salisbury 1979). Based on the mapping of Smith (1958) and Williams (1973) and unpublished maps provided by H. Williams, an average stratigraphic column of the North Arm Massif is given in Fig. 4. The total section is approximately 10 km thick and consists from top to bottom of the following succession:

(1) A thin section of sedimentary rocks consisting of sandy shale and siltstone interbedded with sandy limestone, greywacke and chert.

(2) Relatively fresh pillow lavas, which grade downward into greenschist facies mineral assemblages.

(3) A sheeted dyke section.

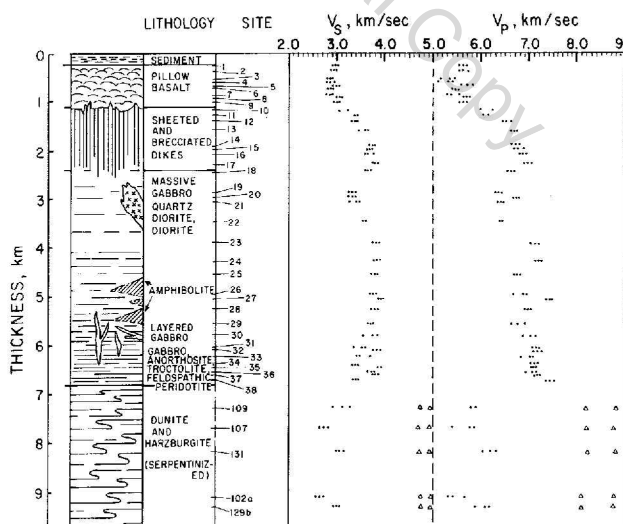

Figure 4. Stratigraphic section of the North Arm massif, Bay of Islands, showing sample location and compressional (V_P) and shear (V_S) wave velocities as a function of depth. The velocities shown as dots are measured values at *in situ* pressures. The triangles represent minimum and maximum velocities calculated from petrofabric analyses for serpentine-free ultramafics (Christensen & Salisbury 1979).

(4) An upper level gabbroic section consisting of massive hornblende gabbro, diorite and quartz diorite.

(5) A lower level gabbro with locally abundant amphibolite and interlayered anorthosite, troctolite and feldspathic peridotite.

(6) Serpentinized dunite and harzburgite tectonite with minor orthopyroxenite.

Our traverses extend across several minor faults, some of which likely originated when the ophiolite was formed. The early map of Smith (1958) shows a major fault (termed the Gregory River fault) extending from the south-west gabbro–ultramafic contact of North Arm Mountain north-west for 12 km, where it swings north-north-east along the Gregory River valley. Within our south-west traverse the fault coincides approximately with the basalt-sheeted dyke contact (Fig. 2) and has been interpreted by Smith (1958) as a high angle reverse fault. The map of Williams (1973) does not show this fault. If the fault does exist, its displacement within the region of our traverse is relatively insignificant for our velocity profiles, since the gradual change in metamorphic grade discussed below continues uninterrupted across this boundary.

The limestone within the sedimentary section is clastic in origin and contains an estimated 70 per cent calcite, 18 per cent quartz and 2 per cent basaltic clasts, with the remainder calcite cement. The siltstones and shales are fine grained, well sorted, contain radiolaria and sponge spicules and are often interbedded with tuffaceous or hyaloclastite layers. The greywackes contain lithic fragments of sandstone, mudstone and basalt in an intergranular matrix of quartz, sericite, calcite, celandonite and opaques.

The extrusive rocks consist of basalts, which often show spectacular pillow structures. The uppermost basalts are relatively fresh with approximately 45 per cent plagioclase (An_{50-55}) and 30 per cent clinopyroxene, with varying proportions of opaques, amygdules and smectite-chlorite. Plagioclase phenocrysts often show oscillatory zoning. The lower portion of the basalt section shows patchy alteration to greenschist facies assemblages consisting of chlorite, actinolite, albite and epidote. Relic clinopyroxene is usually present.

The extrusive rocks are gradational into the sheeted dyke section. Over most of the area the dykes strike NW–SE with nearly vertical dips. In the upper portion of the dyke section, the mineral assemblages are similar to those found in the lower levels of the extrusive sequence. Within the lower dyke section, greenschist facies mineral assemblages are common, as well as epidote–amphibolite mineral assemblages similar to those described in the Blow-Me-Down massif by Salisbury & Christensen (1978). The metamorphic assemblages have overprinted a sub-ophitic igneous fabric and are interpreted as having originated during ocean-floor metamorphism. In addition to relic fabrics, fine-grained chilled margins are often preserved in the dykes. Individual dykes have been observed with two, one, or no chilled margins.

The underlying high-level gabbro is extremely variable in composition. Grain size varies from micro-gabbroic to pegmatitic and compositional layering is rare. The gabbros contain plagioclase with varying proportion of green hornblende and clinopyroxene. Alteration is common, with chlorite, actinolite, prehnite and hydrogrossular often forming major phases. Diorites, quartz diorites and trondhjemites similar to rocks dredged from oceanic regions (Aumento 1969) are also locally abundant in this interval.

The lowermost mafic rocks in the North Arm massif are predominantly medium-grained gabbro and consist of plagioclase (An_{55-65}) and clinopyroxene, with variable amounts of accessory olivine and secondary hornblende, actinolite, chlorite and serpentine. Metamorphism, which is related to introduction of water along fractures and shear zones, has locally produced abundant amphibolite consisting of green hornblende, plagioclase (An_{30-45}) and diopside. The amphibolites vary from massive to well-foliated. The transition from gabbros to ultramafics occurs within a 0.5–1.0 km thick zone of interlayered olivine gabbro, wehrlite and partially serpentinized harzburgite. The rocks in this region have been tectonized by the same process responsible for the metamorphic fabrics in the underlying harzburgites (Christensen & Salisbury 1979).

The lowermost unit consists of pervasively foliated harzburgites with minor dunites and pyroxenites. Banding, produced by a ratio segregation into more dunitic and pyroxenitic layers, is well developed locally. The foliation, which is produced by a planar orientation of the olivine, orthopyroxene and spinels, is generally parallel to the banding. The olivine and orthopyroxene possess strong tectonite fabrics. Serpentinization is common throughout the ultramafic section.

Sample depth locations are shown in Fig. 4, along with the velocity data from Table 1. The measured velocities in the ultramafic rocks are low because of relatively recent serpentinization (Christensen 1972), apparently caused by groundwater. Within the mantle sequence, we also calculated the velocities for serpentine-free ultramafics from petrofabric analyses and olivine single crystal elastic constants (Christensen & Salisbury 1979). Due to strong preferred olivine orientation, these rocks are highly anisotropic, with their magnitude and direction of anisotropy relative to the spreading direction inferred from the sheeted dykes in excellent agreement with the upper mantle anisotropy measured NE of Hawaii (Morris, Raitt & Shor 1969). The paired triangles in Fig. 4 bound the ranges of calculated anisotropies for serpentine-free ultramafic.

In Fig. 5, envelopes defining the ranges in velocities, densities and Poisson's ratios are shown, as well as our best estimate, based on field estimates of the relative abundances of the various lithologies, of the actual velocity structure of the North Arm massif. For estimation purposes, the rocks below the gabbro–ultramafic contact are assumed to be serpentine-free and the rocks at all levels to be free of voids and cracks. For compressional waves, the higher velocity curve in the ultramafics is for horizontal propagation perpendicular to the sheeted dykes (and thus, the ridge crest) and the slower curve is for propagation parallel to the ridge crest. In general, for anisotropic media there are two shear waves which vibrate perpendicular to one another and travel at different velocities for a given propagation direction. The maximum difference in velocity is for propagation parallel to the sheeted dykes

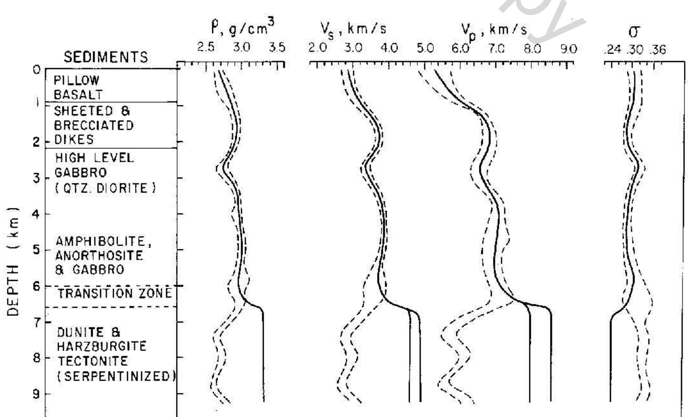

Figure 5. Envelopes of compressional (V_p) and shear (V_s) wave velocity, Poisson's ratio (σ) and density (ρ) versus depth for the North Arm massif. Heavy curves represent best fits to the data. At depths below approximately 7 km, the dashed lines enclose the ranges of measured properties for partially serpentinized ultramafics, whereas the solid curves are calculated from petrofabric studies (Christensen & Salisbury 1979) for serpentine-free rocks.

(Christensen & Salisbury 1979) and is shown in Fig. 5. The velocities of shear waves propagating perpendicular to the dykes fall within these two velocity curves. Poisson's ratios for the crustal section were calculated from the mean velocities of Table 1 and thus are for isotropic aggregates; those shown for the ultramafic section include values calculated in the same manner from measured serpentinite velocities, plus best fit values calculated from averages of the V_p and V_s extremes determined from petrofabric analyses.

The profiles in Fig. 5 have been constructed from core measurements and thus do not include the influence of large-scale fracturing on the properties of the upper section. The presence of fractures within the upper regions of the oceanic crust has been well established by detailed refraction studies (e.g. Houtz & Ewing 1976; Fowler 1976; Whitmarsh 1978; White & Matthews 1980) and by geophysical logging and laboratory studies of basalt velocities of samples obtained from the Deep Sea Drilling Project (e.g. Hyndman & Drury 1976; Kirkpatrick 1979). Although estimates have been made on the overall effect of this fracturing on oceanic crustal velocity profiles (Christensen 1978), the actual distribution of fractures is probably quite variable. Since there is abundant evidence that seawater has penetrated at least to the lower dyke levels of many ophiolites (e.g. Williams & Malpas 1972; Gass & Smewing 1973; Salisbury & Christensen 1978), fracturing in young crust likely extends to depths from the seafloor as great as 5 km.

4 Comparison with the Blow-Me-Down massif

The velocity, density and Poisson's ratio profiles constructed in the preceding section for the North Arm massif are compared in Fig. 6 with similar data obtained from the Blow-Me-Down massif (Salisbury & Christensen 1978). Since seismic anisotropy was not investigated in the ultramafic rocks from Blow-Me-Down, the velocities shown for the ultramafic section of this massif are for isotropic serpentine-free rocks.

In general, the profiles are in excellent agreement, but some important differences exist. In both massifs, the compressional wave velocity increases rapidly from approximately 6.1 to 6.8 km s^{-1} and the shear wave velocity increases from 3.3 to 3.7 km s^{-1} at depths between 1 and 2 km. These increases correlate well in depth and velocity with the layer 2–3 boundary. For both profiles this boundary originates, in part, from increasing metamorphic grade. The lower-velocity dyke rocks contain greenschist facies mineral assemblages, whereas the dyke rocks with velocities above 6.5 km s^{-1} generally contain amphibolite facies mineral assemblages.

Several observations suggest that the metamorphism primarily responsible for the velocity gradients within the basalts and dyke rocks did not originate from an overprint associated with emplacement of the ophiolite on land. First, the sedimentary rocks and pillow basalts which form the uppermost few hundred metres of the section are unmetamorphosed. Second, the metamorphic rocks from the basalt and dyke sections of the ophiolite have mineral assemblages and textures similar to those reported from dredged oceanic metamorphics (e.g. Bonatti, Horrorez & Ferrara 1970; Miyashiro, Shido & Ewing 1971). Also, the metamorphic grade within the ophiolite section increases with depth (Williams & Malpas 1972; Salisbury & Christensen 1978) consistent with thermal models expected near ridge crests (e.g. Oxburgh & Turcotte 1968).

Another factor, previously unrecognized, which is partially responsible for the rapid increase in velocity with depth within the sheeted dyke section is a corresponding decrease in grain boundary porosity. This factor is illustrated in Fig. 7, in which the average porosities of the dyke rocks shown in Table 1 (samples 10–17) are plotted against mean velocities at 1 kbar confining pressure; since the porosities tend to decrease with depth within the dykes,

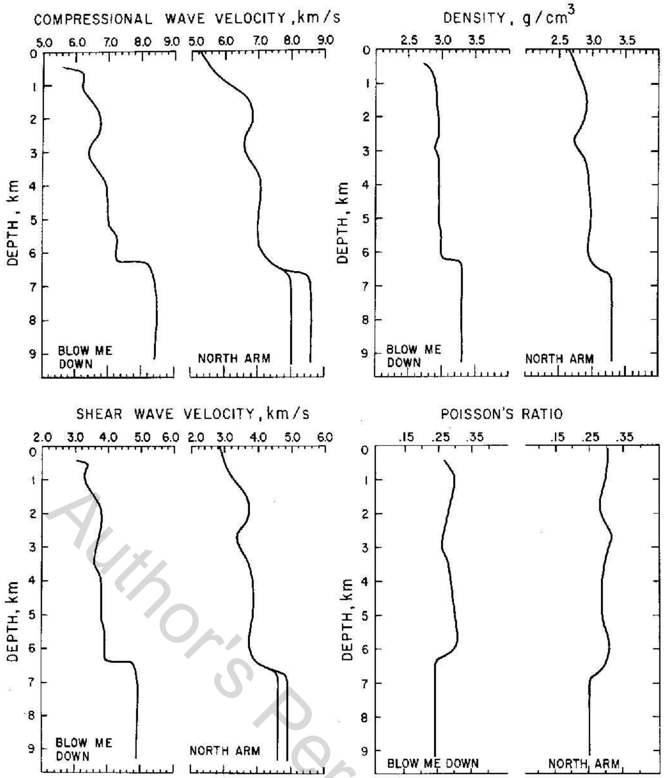

Figure 6. Comparisons of velocity, density, and Poisson's ratio versus depth for the North Arm and Blow-Me-Down massifs. Ranges of velocities originating from anisotropy of unserpentinized ultramafics are shown for the North Arm velocity profiles.

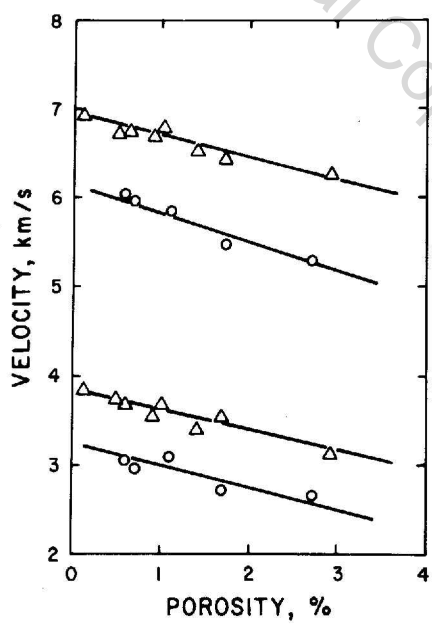

Figure 7. Mean compressional and shear wave velocities at 1 kbar versus porosities for dyke rocks (triangles) and serpentinized peridotites (circles) from the North Arm massif.

Table 2. Measured effective porosities.

Unit	Samples	Porosity (%)	
		Range	Mean
Pillow Basalt	1-9	0.8-3.3	2.1
Dikes	10-17	0.1-2.9	1.1
High Level Gabbro	18-24	0.5-0.9	0.7
Lower Gabbro	27, 29, 30 32, 34 -38	0.1-0.8	0.3
Serpentinized Peridotite	109, 107, 131, 102A, 129b	0.6-2.7	1.4

the velocities must increase. Also shown are porosity–velocity data for partially serpentinized peridotites from the base of the section; although the data show a similar trend, they do not imply the presence of a velocity gradient since the porosity varies randomly with depth at this level and is strongly influenced by post-emplacement serpentinization. It is also interesting to note in this context that the average grain boundary porosity of the various lithological units tends to decrease with depth in the complex (Table 2). Even at atmospheric pressure, for example, the average porosity of the gabbros at the base of the crustal section is only one-seventh that of the basalts near the surface.

Within the Blow-Me-Down massif, the presence of high-velocity pumpellyite gave rise to relatively high basalt velocities between 0.5 and 1.0 km of the surface. Although locally present in rocks from the North Arm traverse, pumpellyite is not nearly as abundant; thus the uppermost velocities for this massif are significantly lower.

Within the high level gabbros between 2 and 4 km, both massifs show a marked compressional wave velocity inversion and a density minimum. In many ophiolites, this region contains pods, dykes and sills of quartz-bearing plagiogranite (Coleman & Peterman 1975), displaying relatively low velocities and a low Poisson's ratio (Salisbury & Christensen 1978; Christensen 1978). The high level gabbros are also commonly altered by deuteric processes so that they contain chlorite, prehnite, uralite, and hydrogrossular. Although plagiogranites are rare, deuteric alteration is particularly common in the North Arm section, causing the rocks at this level to have high Poisson's ratios (0.31–0.34). Thus the North Arm velocity profile has an increase in Poisson's ratio between 2 and 3 km depth, whereas the Poisson's ratio decreases with depth in the Blow-Me-Down massif because of the presence of greater volumes of plagiogranite along our traverse.

Velocities within the lower crustal sections (between 4 and 7 km) of the two profiles also show significant differences. At a depth of 5.3 km in the Blow-Me-Down massif, we found a step increase in compressional wave velocity from 7.0 to 7.4 km s^{-1}. This velocity correlates well with the crustal high-velocity basal layer commonly found in airgun refraction profiles (Sutton, Maynard & Hussong 1971) and originates from an increase in modal olivine. This seismic feature, however, is not present in our North Arm profile, where slight decreases in velocity are observed at depths in the vicinity of 6 km. These inversions would be further accentuated if the effects of temperature were taken into account (Christensen 1979).

Due to the 0.5–1.0 km thick mixed zone of gabbro, wehrlite, and harzburgite along the crust–mantle contact in the North Arm massif, the velocity transition is somewhat more gradual for our North Arm velocity profiles. The mafic–ultramafic contact on Blow-Me-Down, on the other hand, is relatively sharp because of faulting. Thus the velocity structure for North Arm in the 6–7 km depth interval is likely to be more representative of the oceanic Mohorovičić discontinuity.

5 Discussion and conclusions

Based on our earlier velocity profile of the Blow-Me-Down massif and on the present study, we conclude that the velocity structure of the Bay of Islands ophiolite complex is indistinguishable from that of normal oceanic crust. Early three-layered seismic models of the oceanic crust (Raitt 1963) consisted of a thin sediment veneer underlain by a 1.0–2.5 km thick basement (layer 2) having compressional wave velocities commonly between 4.4 and 5.6 km s^{-1}, and a 4–5 km thick oceanic layer (layer 3) with velocities commonly between 6.4 and 7.0 km s^{-1}. These models are consistent with the velocity profiles in Fig. 6. More recently, a series of multiple-layered models based on sonobuoy and OBS data have been proposed (Sutton *et al.* 1971; Houtz & Ewing 1976). These, in turn, have evolved into detailed gradient models derived from velocity and amplitude analyses of reflection and refraction data (Helmberger & Morris 1970; Orcutt, Kennett & Dorman 1976; Malacek & Clowes 1978). Our laboratory profiles support the gradient models and show remarkable similarity to several recently published examples (Malacek & Clowes 1978; Spudich, Salisbury & Orcutt 1978).

Since the Bay of Islands ophiolite complex appears to be indistinguishable from normal oceanic crust in terms of its velocity structure along widely spaced traverses, it follows that the seismic structure of the oceanic crust may be interpreted in terms of petrology through correlation of the velocity and petrologic columns of the complex.

The petrologic conclusions reached in this paper are essentially similar to those summarized earlier from our study of the Blow-Me-Down massif (Salisbury & Christensen 1978), but with the following additional observations:

(1) Strong positive velocity gradients exist within the upper 2 km of the oceanic crust beneath the sediment cover. Two major interrelated factors responsible for these gradients are decreasing grain boundary porosity and increasing metamorphic grade with depth. If the effects of intercalated sediments, pillow interstices, pore pressure and water-filled cracks and joints were taken into account, the gradients produced would undoubtedly be more pronounced than those shown in Fig. 6.

(2) A major low-velocity zone associated with a region of low density occurs at depths of between 2 and 4 km. There are multiple origins for this zone: when due to quartz-rich plagiogranite intrusions, the compressional wave velocity decreases more than the shear wave velocity giving rise to low values of Poisson's ratio (0.25–0.27); if caused by deuteric alteration of high level gabbros, V_s decreases proportionately more than V_p, giving rise to relatively high Poisson's ratios (0.31–0.34).

(3) Within the Blow-Me-Down massif, the lower crust displays relatively high velocities ($V_p \simeq 7.4$ km s^{-1}; $V_s \simeq 3.9$ km s^{-1}) in agreement with the observations of Sutton *et al.* (1971). Lateral heterogeneity within this region is demonstrated by the absence of a high-velocity basal layer in the North Arm massif. Our velocity profiles have not taken into account the lowering of velocity with depth produced by increasing temperatures. Thus a velocity inversion is likely within this region as suggested by Lewis & Snydsman (1977) on the basis of seismic data for these depths. However, the origin of the velocity inversion is quite different from their proposed model, which is based on serpentinization.

(4) Due to the interlayering of gabbro and ultramafic rocks, the crust–mantle boundary is likely to be spread out over a greater depth interval than in our previous estimate. It was shown earlier from petrofabric and petrographic observations (Christensen & Salisbury 1979) that upper mantle deformation originating from plate motion extended through this transition region into the lower crustal section. Thus seismic anisotropy is present throughout the ultramafic section and continues, though much smaller in magnitude, upward into the gabbros.

A possible explanation for the heterogeneity is lateral variation in the sizes and levels of emplacement of lower crustal magma chambers under spreading centres. Although magma chamber models for the formation of oceanic crust based on the presence of single large chambers may be locally applicable, we suggest that in actuality the configuration is exceedingly more complex.

Although the essential features of our earlier petrologic interpretation of oceanic seismic structure have been confirmed in this study, it is only by reconstructing the velocity of the crust along many such traverses that general patterns of petrologic control over velocity can be convincingly distinguished from local variations. From a comparison of the traverses completed to date, it is already clear that much of the variation observed in oceanic seismic structure can be explained in terms of local differences in petrology and structure. Given the number and influence of the variables which have operated in the crust, the alleged homogeneity of the crust deduced from early seismic studies can only be a relict of seismic averaging. With increasingly sophisticated seismic data and a better understanding of the velocity structure of the ophiolites, it is becoming apparent that lateral heterogeneity is an inherent feature of the ocean crust.

Acknowledgments

We wish to thank H. Williams for his encouragement and support of this study. Financial support was provided by the Office of Naval Research, Contract N-00014-80-C-0252.

References

Aumento, F., 1969. Diorites from the mid-Atlantic ridge at 45° N, *Science*, **165**, 1112–1113.

Birch, F., 1960. The velocity of compressional waves in rocks to 10 kilobars, 1, *J. geophys. Res.*, **65**, 1083–1102.

Bonatti, E., Honnorez, J. & Ferrara, G., 1970. Equatorial mid-Atlantic ridge: petrologic and Sr isotopic evidence for an alpine type rock assemblage, *Earth planet. Sci. Lett.*, **9**, 247–256.

Christensen, N. I., 1972. The abundance of serpentinites in the ocean crust, *J. Geol.*, **80**, 709–719.

Christensen, N. I., 1978. Ophiolites, seismic velocities and oceanic crustal structure, *Tectonophys.*, **47**, 131–157.

Christensen, N. I., 1979. Compressional wave velocities in rocks at high temperatures and pressures, critical thermal gradients, and crustal low-velocity zones, *J. geophys. Res.*, **84**, 6849–6857.

Christensen, N. I. & Salisbury, M. H., 1975. Structure and constitution of the lower oceanic crust, *Rev. Geophys. Space Phys.*, **13**, 57–86.

Christensen, N. I. & Salisbury, M. H., 1979. Seismic anisotropy in the oceanic upper mantle: Evidence from the Bay of Islands ophiolite complex, *J. geophys. Res.*, **84**, 4601–4610.

Church, W. R. & Stevens, R. K., 1971. Early Paleozoic ophiolite complexes of the Newfoundland Appalachians as mantle–oceanic crust sequences, *J. geophys. Res.*, **76**, 1460–1466.

Coleman, R. G. & Peterman, Z. E., 1975. Oceanic plagiogranite, *J. geophys. Res.*, **80**, 1099–1108.

Cooper, J. R., 1936. Geology of the southern half of the Bay of Islands Igneous Complex, *Bull. Newfoundland Rep. Nat. Res., Geol. Sect., No. 4*, 62 pp.

Fowler, C. M. R., 1976. Crustal structure of the Mid-Atlantic ridge crest at 37N, *Geophys. J. R. astr. Soc.*, **47**, 459–492.

Gass, I. G. & Smewing, J. D., 1973. Intrusion, extrusion and metamorphism at constructive margins: evidence from the Troodos massif, Cyprus, *Nature*, **242**, 26–29.

Helmberger, D. V. & Morris, G. B., 1970. A travel time and amplitude interpretation of a marine refraction profile: transformed shear waves, *Bull. seism. Soc. Am.*, **60**, 593–600.

Houtz, R. & Ewing, J., 1976. Upper crustal structure as a function of plate age, *J. geophys. Res.*, **81**, 2490–2498.

Hyndman, R. D. & Drury, M. J., 1976. The physical properties of oceanic basement rocks from deep drilling on the mid-Atlantic ridge, *J. geophys. Res.*, **81**, 4042–4052.

Jacobsen, S. B. & Wasserburg, G. J., 1979. Nd and Sr isotopic study of the Bay of Islands ophiolite complex and the evolution of the source of mid-ocean ridge basalts, *J. geophys. Res.*, **84**, 7429–7445.

Karson, J. & Dewey, J. F., 1978. Coastal complex, western Newfoundland: an early Ordovician oceanic fracture zone, *Bull. geol. Soc. Am.*, **89**, 1037–1049.

Kirkpatrick, R. J., 1979. The physical state of the oceanic crust: results of downhole geophysical logging in the mid-Atlantic ridge at 23N, *J. geophys. Res.*, **84**, 178–188.

Lewis, B. T. R. & Snydsman, W. E., 1977. Evidence for a low velocity layer at the base of the ocean crust, *Nature*, **266**, 340–344.

Malacek, S. J. & Clowes, R. M., 1978. Crustal structure near Explorer Ridge from a marine deep seismic sounding survey, *J. geophys. Res.*, **83**, 5899–5912.

Mattinson, J. M., 1976. Ages of zircons from the Bay of Islands ophiolite complex, western Newfoundland, *Geology*, **4**, 393–394.

Miyashiro, A., Shido, F. & Ewing, M., 1971. Metamorphism in the mid-Atlantic ridge near 24° and 30° N, *Phil. Trans. R. Soc. A*, **268**, 589–603.

Morris, G. B., Raitt, R. W. & Shor, G. G., 1969. Velocity anisotropy and delay-time maps of the mantle near Hawaii, *J. geophys. Res.*, **74**, 4300–4316.

Orcutt, J. A., Kennett, B. L. N. & Dorman, L. M., 1976. Structure of the East Pacific Rise from an ocean bottom seismometer survey, *Geophys. J. R. astr. Soc.*, **45**, 305–320.

Orcutt, J. A., Kennett, B., Dorman, L. & Prothero, W., 1975. Evidence for a low velocity zone underlying a fast-spreading rise crest, *Nature*, **256**, 475–476.

Oxburgh, E. R. & Turcotte, D. L., 1968. Mid-ocean ridges and geotherm distribution during mantle convection, *J. geophys. Res.*, **73**, 2643–2661.

Raitt, R. W., 1963. The crustal rocks, in *The Sea*, **3**, 85–102, ed. Hill, M. N., Wiley, New York.

Salisbury, M. H. & Christensen, N. I., 1978. The seismic velocity structure of a traverse through the Bay of Islands ophiolite complex, Newfoundland: an exposure of oceanic crust and upper mantle, *J. geophys. Res.*, **83**, 805–817.

Smith, C. H., 1958. Bay of Islands igneous complex, western Newfoundland, *Mem. geol. Surve. Can., 290.*

Spudich, P. K. P., Salisbury, M. H. & Orcutt, J. A., 1978. Ophiolites found in oceanic crust?, *Geophys. Res. Lett.*, **5**, 341–344.

Stevens, R. K., 1970. Cambro-Ordovician flysch sedimentation and tectonics in west Newfoundland and their possible bearing on a proto-Atlantic ocean, in *Flysch Sedimentology in North America*, pp. 165–177, ed. Lajoie, J., *Spec. Pap. 7, geol. Ass. Can.*, Waterloo, Ontario, Canada.

Sutton, G. H., Maynard, G. L. & Hussong, D. M., 1971. Widespread occurrence of a high-velocity basal layer in the Pacific crust found with repetitive sources and sonobuoys, in *The Structure and Physical Properties of the Earth's Crust*, pp. 193–209, ed. Heacock, J. G., *Geophys. Monogr. Ser. Am. geophys. Un.*, **14**, Washington, DC.

White, R. S. & Matthews, D. H., 1980. Variations in oceanic upper crustal structure in a small area of the north-eastern Atlantic, *Geophys. J. R. astr. Soc.*, **61**, 401–436.

Whitmarsh, R. B., 1978. Seismic refraction studies of the upper igneous crust in the North Atlantic and porosity estimates for layer 2, *Earth planet. Sci. Lett.*, **37**, 451–464.

Williams, H., 1971. Mafic–ultramafic complexes in western Newfoundland Appalachians and the evidence for transportation: a review and interim report, *Proc. geol. Ass. Can.*, **24**, 9–25.

Williams, H., 1973. The Bay of Islands map area, Newfoundland, *Geol. Surv. Can. Pap., 72-34*, 1–7.

Williams, H., 1975. Structural succession, nomenclature, and interpretation of transported rocks in western Newfoundland, *Can. J. Earth Sci.*, **12**, 1874–1894.

Williams, H. & Malpas, J., 1972. Sheeted dikes and brecciated dike rocks within transported igneous complexes, Bay of Islands, western Newfoundland, *Can. J. Earth Sci.*, **9**, 1216–1229.

Wilson, J. T., 1966. Did the Atlantic close and then reopen?, *Nature*, **211**, 676–681.